Progress Report of KRISS on DC, LF, RF and Magnetic Measurement (2021-2022)

DCLF: Hyung-Kew Lee (hyungkew.lee@kriss.re.kr)
RF: Jae-Yong Kwon (jykwon@kriss.re.kr)

1. Quantum Hall Resistance in Closed-Cycle Cryomaget (Dr. Dong-Hun Chae)

Graphene-based quantum Hall resistance in a closed-cycle cryomagnet (B= 7 T and T=3 K) is realized. We have confirmed that the degree of equivalence between KRISS GaAs-QHR standard at 0.3 K and 9.5 T and graphene-based QHR at 3 K and 5 T is smaller than 5 nΩ/Ω. We plan to combine this system with a direct current comparator (DCC) for calibration service with a target uncertainty of 20 nΩ/Ω. We also plan to use this system for the impedance traceability.

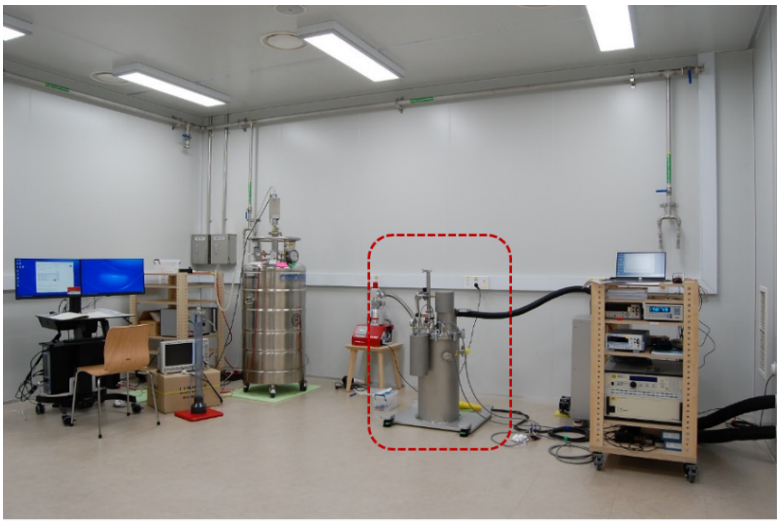

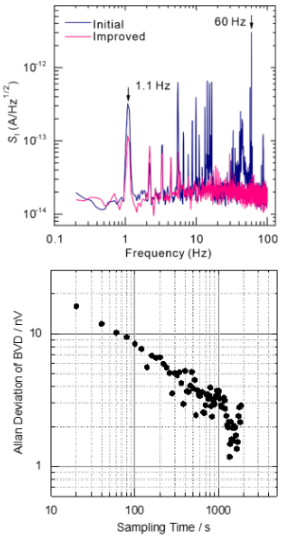

2. Digital Bridge up to 100 kHz (Dr. Dan Bee Kim, Dr. Wan-Seop Kim, Dr. Jan Kucera)

A digital coaxial bridge was evaluated for its frequency extension up to 100 kHz. The bridge can be configured in difference modes of either digitally assisted (DA) or fully digital (FD). The 10:1 capacitance ratio of 1000 pF:100 pF measurements were performed then compared with the reference values obtained using the Z-matrix method. The measurement results showed that the bridge accuracy could reach 10^{-5} level at the highest frequency of 100 kHz for the bridge modes of DA and FD with injection.

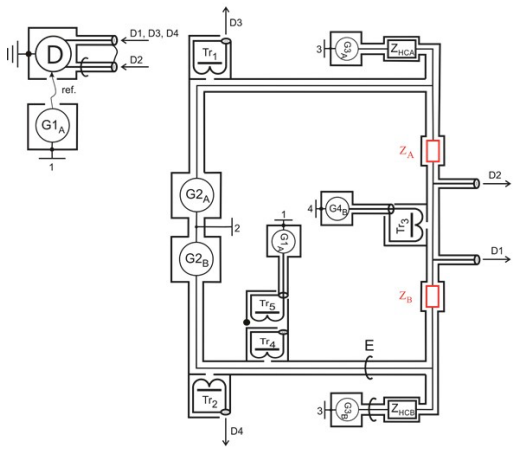

Fully Digital Bridge with Voltage Injection

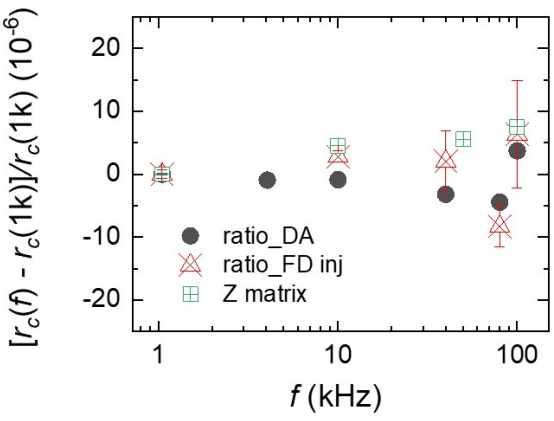

1000 pF:100 pF capacitance ratio against the frequency

3. PJVS-based differential sampling of AC Voltage (Dr. Mun-Seok Kim)

KRISS joined a pilot study for an on-site comparison of AC voltage measurement based on a PJVS-based differential sampling proposed by the BIPM in 2015. BIPM, KRISS, and PTB carried out comparisons in a frequency range below 1 kHz using the PJVS systems and sampling systems developed in BIPM, NIST, PTB, and KRISS at the PTB in Braunschweig. In the study, comparisons using three types of samplers with different filters (Keysight 3458A, NI PXI-5922, and Fluke 8588A) were conducted for the first time. One of the main purposes of this study was to investigate the effect of the transfer function of the filter for the samplers on the measurement result.

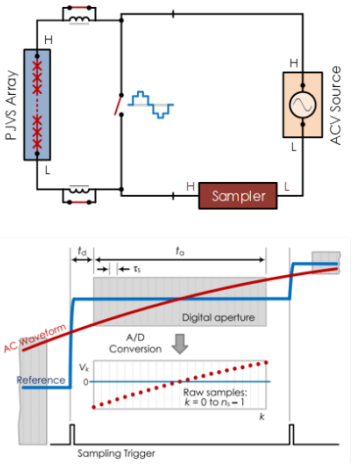

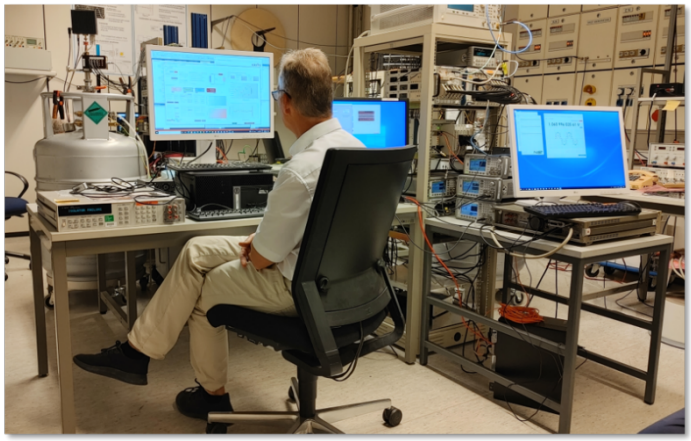

4. Apparent Charge Measurement for Partial Discharge Calibrator (Dr. Jin-Hyeok Kim and Dr. Hyung-kew Lee)

An apparent charge measurement system has been developed to quantify the amount of partial discharge(PD) injected from a commercial PD calibrator. The PD pulse is measured based on resistor-based method from IEC 60270 and digitized by a digital oscilloscope. At the same time, a multifunction calibrator is used to evaluate and compensate possible offsets in the measured voltage value. Uncertainty analysis is being conducted to provide calibration services for partial discharge generators from 2023.

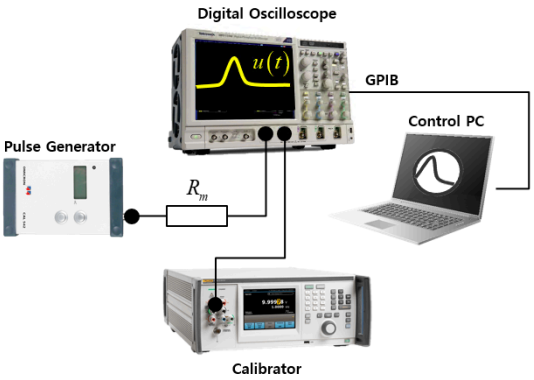

Apparent charge measurement system

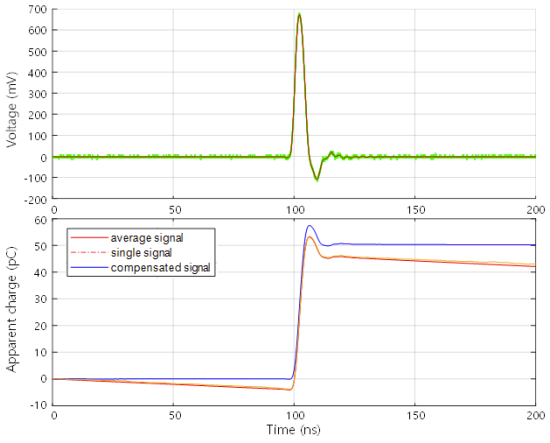

(Top) PD pulse from pulse generator
(Bottom) Apparent charge evaluation

5. DC Energy Standard for fast EV chargers (Dr. Kyu-Tae Kim and Dr. Hyung-Kew Lee)

The capacity and number of fast EV charger in Korea are rising significantly recently. As a result, DC energy has been included in legal metrology in Korea since January of 2020. KRISS developed DC energy standard for the validation of fast EV chargers up to 500 kW (1000 V, 500 A) to fulfill the demand from the society. The calibration uncertainty of the developed standard is 0.02 % (k = 2) for 500 kW charging power. Calibration service for reference energy meters (ZERA COM 3003) is currently being provided to testing laboratories.

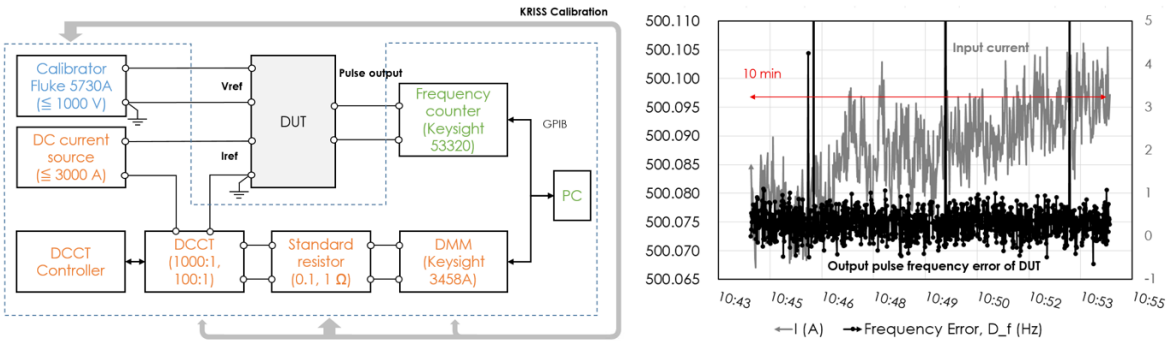

6-1. Precision measurement of parallelized single electron pumps (Dr. Myung-Ho Bae, Dr. Bum-Kyu Kim, Dr. Nam Kim, Dr. Wan-Seop Kim)

(a) False-color scanning electron microscope image of parallelized five pumps (P1-P5) with three gates (G1-G3) crossing the pumps. The light blue and green regions indicate non-etched and etched regions, respectively. An rf single is added on G1. (b) I-VG3 curves of P1 (solid black curve), P2 (blue curve) and P1&P2 (red curve) in a parallel mode at VG1 = −0.28 V, VG2 = −0.506 V, f = 0.17 GHz (Prf = 1 dBm), B = 10.2 T and T = 0.45 K. (c) Precision measurement results, $\langle \delta I_3 \rangle$ as a function of VG3 with various Ncyc with error bars for the parallel mode. $\delta I_n = (-I - nef)/nef$. A cyan curve predicted by the decay cascade model is added for the comparison. we perform a long-term measurement process at two points of VG3 = −0.457 and −0.458 V, which give relative deviations from 3ef with type-A uncertainties (uA) of $(-0.34 \pm 0.89) \times 10^{-6}$ and $(0.75 \pm 0.86) \times 10^{-6}$, respectively. Then, we obtain an averaged deviation value of the two points as $(0.24 \pm 0.66) \times 10^{-6}$ with a combined uncertainty ($\sqrt{u_A^2 + u_B^2}$). Here, $u_B (= 0.23 \times 10^{-6})$ is a type B (systematic) uncertainty.

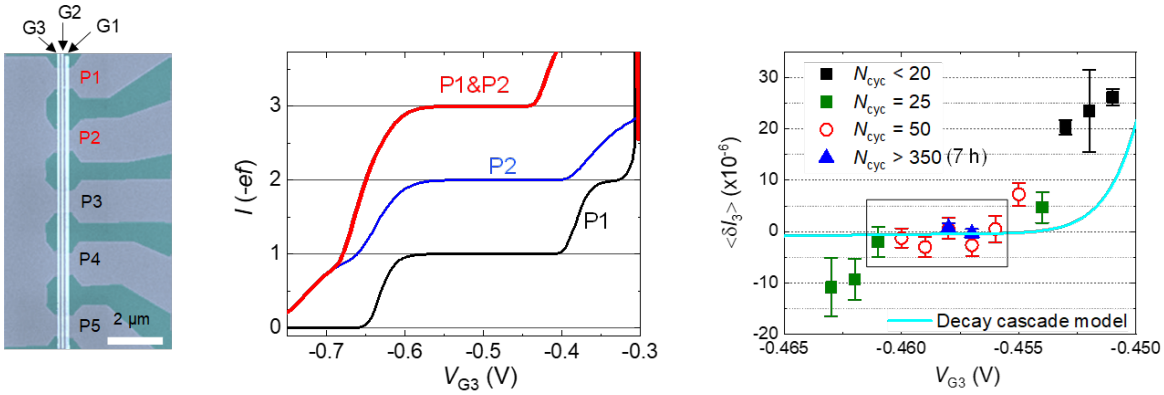

6-2. Evaluation of single-electron current with CCC and QHR (Dr. Wan-Seop Kim, Dr. Young-Seok Ghee, Dr. Bum-Kyu Kim, Dr. Nam Kim, Dr. Myung-Ho Bae)

(a) Schematic diagram for evaluation of single-electron current with CCC and QHR. The single-electron pump (SEP) current, amplified by the CCC was fed into QHR device and the Hall voltage across the QHR device was measured by a digital voltmeter. (b) Bipolar SEP current of ±0.4 nA generated over the exit gate voltage between 0.22 V ~ 0.28 V by control of the bipolar (BP) gate voltages. To change polarity of the SEP current in coincident with the CCC, the SEP BP gate voltage was controlled by a sync signal of the CCC (c, top). The following current (c, bottom) was amplified by the CCC with a gain of 10^3. (d) Offset voltage of -18.3 μV measured at a closed exit gate (SEP current 0). (e) The calculated current of ±1.055 nA from the Hall voltage measurement of 27.242 mV shows a large deviation possibly caused by feedback current of the CCC.

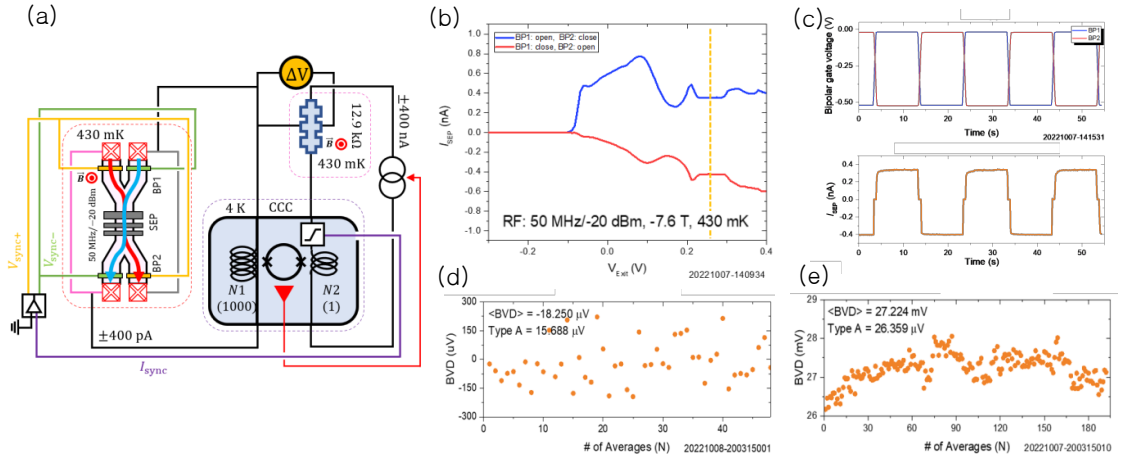

7. RF Impedance (Dr. Chi-Hyun Cho, Dr. Hyunji Koo, Dr. Tae-Weon Kang, Dr. Jae-Yong Kwon)

We have measured the airline dimensions from the PTB. From those dimensions, we established 2.4 mm impedance standards. We constructed a residual model from the calibration kit uncertainty. This model has the same uncertainty results as the conventional VNA model. All impedance calibration services have been changed to residual models. KRISS started calibration service from 9 kHz for N-type, 3.5 mm, 2.92 mm, and 2.4 mm in 2022. We have established D-band impedance and finished the peer review in 2022. New CMC tables for coaxial impedance (Type-N, 3.5 mm, 2.92 mm, 2.4 mm) and V- and D-bands will be updated. And we plan to provide E-cal calibration service from 2023. We completed the measurement setup for material characterization of Q-, V-, W-, D-, and J-band. The research on wafer impedance on D-band is in progress. Soon, we plan to have the reliability of the measured values through comparison with PTB.

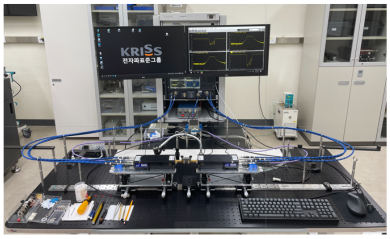

Waveguide impedance measurement system

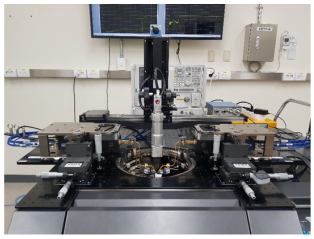

On-wafer measurement system

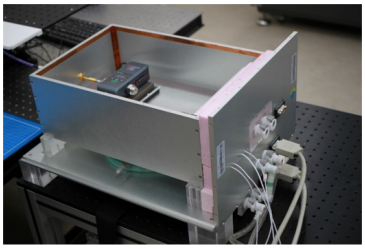

Characterization of E-cal. kit

8. RF power (Dr. Jae-Yong Kwon)

We set up and evaluated a D-band (110 GHz ~ 170 GHz) waveguide power calibration system (direct comparison system). We are preliminarily evaluating KRISS transfer standards and commercial power meters using the system.

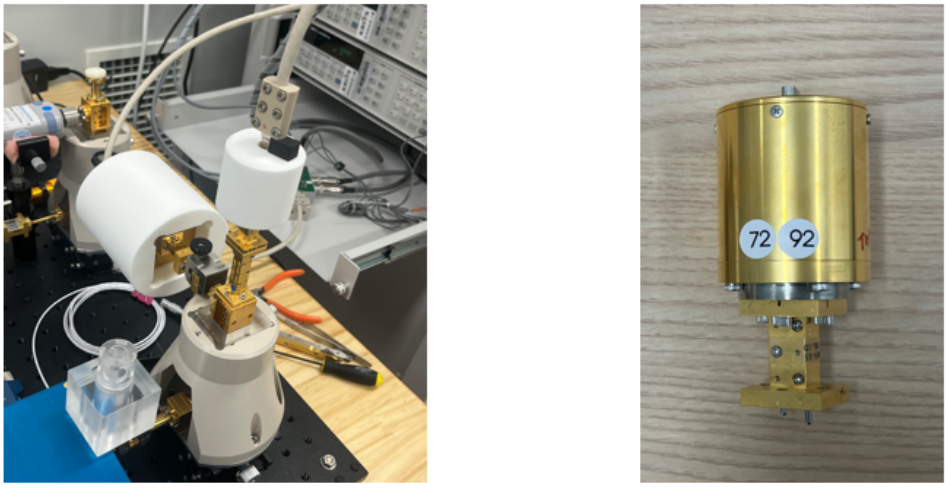

KRISS D-band direct comparison system and transfer standard

8. Attenuation (Dr. Joo-Gwang Lee)

We have developed a low frequency attenuation system operating at 9 kHz to 10 MHz. An evaluation of the uncertainty was conducted and peer-reviewed. CMC is 0.007 dB ~ 0.083 dB (k=2) in the attenuation range of 0.01 dB ~ 100 dB.

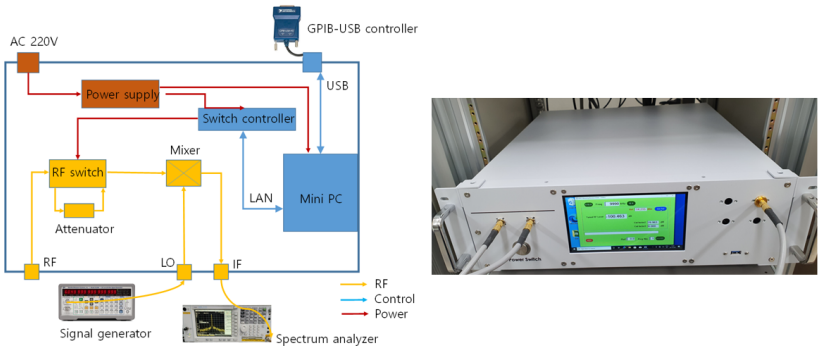

Low frequency attenuation measurement system

9. Field strength (Dr. Young-Pyo Hong and Dr. Dong-Joon Lee)

We constructed a measurement system capable of not only rotating the azimuth angle of the probe but also changing the separation distance between the antenna and the probe. The uncertainty of the components providing traceability to the system was also evaluated. The system is expected to generate a standard field higher than 10 V/m in Ka-band (26.5–40 GHz). Uncertainty in the correction factors is quantified to determine the factors that affect the calibration, and the expanded uncertainty of the standard field generation system is evaluated to be 5.1% at 26.5 GHz and 5.3% at both 33 and 40 GHz. Moreover, for partial validation of the standard field generation system, the system is configured for K-band (18–26.5 GHz) and Ka-band with the same electric-field probe, after which their correction factor results are compared at the overlapping frequency, 26.5 GHz.

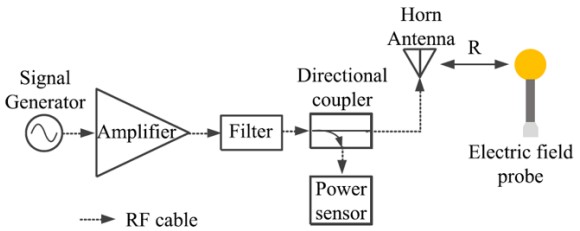

Measurement system

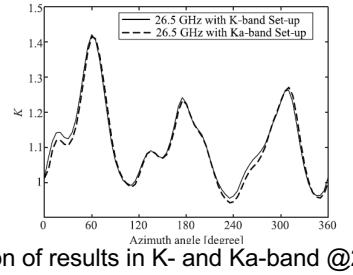

Comparison of results in K- and Ka-band @26.5 GHz

We have developed field-calibrated electrooptic probes designed for millimeter-wave (mm-wave) 5G phased array antenna and Ka-band(26.5~40 GHz) rectangular waveguide. The fabricated probes are specifically minute enough to fit inside a standard mm-wave waveguide section for calibration in a minimally invasive way. The proposed calibration method is validated by analyzing the field invasiveness and through a simulation. Electric field distributions with an absolute V/m scale from an mm-wave antenna are presented using a calibrated probe associated with a heterodyning probe control system.

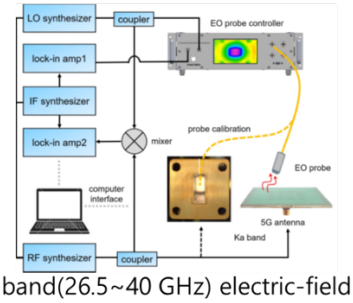

Ka-band(26.5~40 GHz) electric-field calibration system using electro-optic system

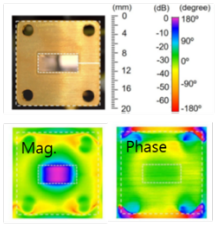

E-field images for WR-28 at 28 GHz

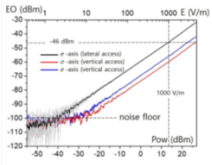

field-calibrated EO probe

10. Antenna (Jeong-Il Park and Dr. In-June Hwang)

A measurement system for a Q-band (33~50 GHz) antenna is developed. The performance of the Q-band antenna measurement system is evaluated by measuring the far-field gain of an electroformed standard gain horn antenna.

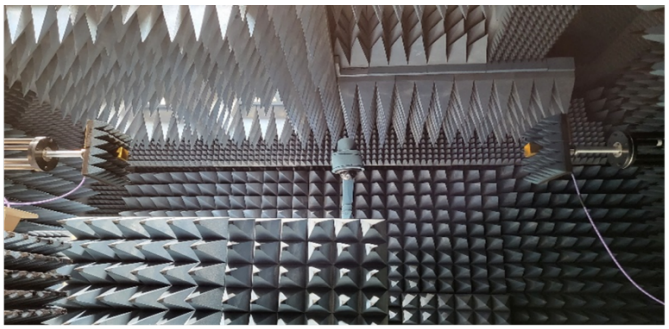

Q-band(33~50 GHz) antenna measurement system in anechoic chamber